

We are IntechOpen, the world's leading publisher of Open Access books Built by scientists, for scientists

4,800

Open access books available

122,000

International authors and editors

135M

Downloads

Our authors are among the

154

Countries delivered to

TOP 1%

most cited scientists

12.2%

Contributors from top 500 universities



WEB OF SCIENCE™

Selection of our books indexed in the Book Citation Index
in Web of Science™ Core Collection (BKCI)

Interested in publishing with us?
Contact book.department@intechopen.com

Numbers displayed above are based on latest data collected.
For more information visit www.intechopen.com



Voltage Regulation in Smart Grids

Maher Azzouz

Abstract

The intermittent nature of renewable power sources (RES) can significantly change the voltage profile of smart grids and adversely impact the conventional voltage control devices such as tap-changing transformers and capacitor banks. Furthermore, the growing penetration of plug-in electric vehicles (PEVs) can add high stress on voltage control devices due to the PEV stochastic and concentrated power profiles. Such power profiles may lead to high maintenance costs and reduced lifetimes for voltage control devices and limit actions on accommodation of high penetration levels of RES and PEVs. This chapter explains the basic background of voltage regulation in smart grids. The typical approaches, which are employed by utilities for voltage regulation, are reviewed. Then, the impact of RES and PEVs on voltage regulation is analyzed. Lastly, remedies for voltage violations in smart grids, such as optimal reactive power control and coordination between voltage control devices, are discussed.

Keywords: distributed generation, active distribution networks, voltage regulation, electric vehicles, onload tap changers

1. Introduction

Ongoing rapid advances in power electronics and communication technologies are facilitating the development of smart grids that are characterized by hosting distributed generation units (DGs). There are many benefits of smart grids such as enhancing power reliability and power quality, improving safety and cyber security, maximizing energy utilization and efficiency, environment protection and conservation, and increasing financial revenues [1]. For instance, as reported in [2], smart grids could reduce greenhouse gas emissions by up to 18%. The integration of renewable-based DGs alters distribution systems so that rather than having passive structures, with unidirectional power flow, they become active distribution networks (ADNs), with multidirectional power flow. Voltage regulation is considered one of the main operational challenges that accompany high penetration levels of renewable-based DGs. RES, such as wind and solar energy, can significantly change the voltage profile of smart grids and interact negatively with conventional schemes of controlling onload tap changers (OLTCs). Another factor is the growing penetration of PEVs, which creates additional stress on voltage control devices due to their stochastic and concentrated power profiles. These combined generation and load power profiles can lead to overvoltages, undervoltages, high system losses, excessive tap operation, infeasible solutions (hunting) with respect to OLTCs, and/or limits on the integration of either PEVs or RES.

2. Background

One of the main objectives of electric utilities is to maintain the grid voltage within standard levels to guarantee customers' satisfaction. Many equipment are deployed in the grid, such as OLTCs and capacitor banks, to properly fulfill this objective. In general, voltage regulation in a smart grid can be classified as local or communication-assisted [3]. The local voltage regulation is referred to as the conventional control, where the reference values and measurements for voltage control are locally determined. In this section, the fundamentals of the conventional control of OLTC and inverter-interfaced DGs are explained.

2.1 OLTC conventional controller

OLTCs are one of the main voltage regulators in distribution systems. A tap changer equipped with an automatic control system usually regulates the transformer's secondary voltage to maintain an acceptable voltage near the load center. The tap changer mechanically varies the tap position from zero (no voltage compensation) to N_{max} (maximum voltage compensation). This allows for changing the transformer's turn ratio in discrete steps; each step adjustment may take 3–20 seconds. **Figure 1** displays the schematic diagram of an OLTC, where the tap changer is placed on the primary side. The tap changer is usually installed on the high voltage side of the transformer (i.e., the primary side in **Figure 1**) because of the low current of that side. A reversing switch is employed to change the polarity of the tap winding for positive and negative voltage compensation. In steady state, the transformer model can be given by

$$V_2 = \frac{V_1}{a} - I_2 Z_T(a) \quad (1)$$

where V_1 and V_2 are primary and secondary voltages, respectively, I_2 is secondary current, a denotes the transformer's tap ratio, and $Z_T(a)$ is the transformer

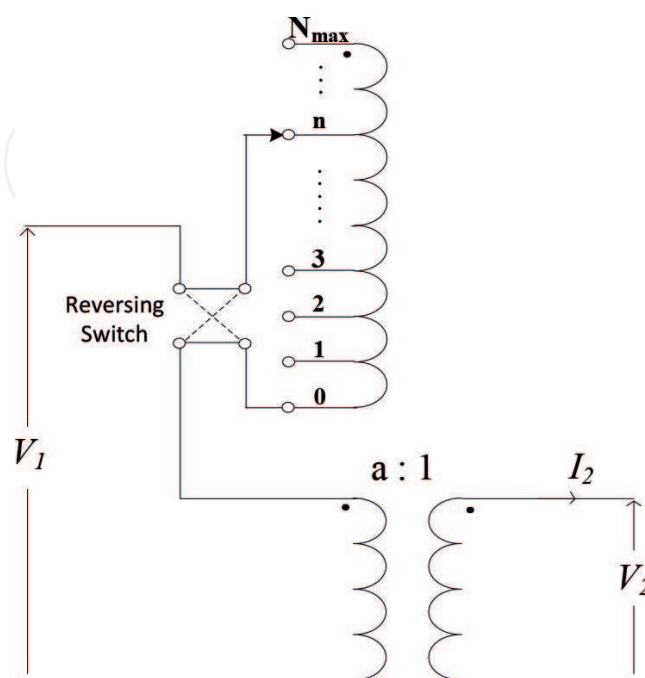


Figure 1.
Transformer with tap changer.

series impedance (referred to the secondary side). The tap changer allows a to vary linearly; thus it can be expressed in terms of the nominal turn ratio (i.e., $a_0 = 1.0$):

$$a = a_0 + n_i \Delta a \quad (2)$$

where Δa is the change in a as a result of a step change in the tap position n_i , which is given by

$$n_i = n_{i-1} + \Delta n \quad (3)$$

where n_i is the present tap position and n_{i-1} is the previous tap position. Δn is the change in the tap position which is defined by

$$\Delta n = \begin{cases} 0 & \text{for } t \leq T_m : b = \text{arbitrary} \\ 1 & \text{for } t > T_m : b = -1 \\ -1 & \text{for } t > T_m : b = 1 \end{cases} \quad (4)$$

where T_m denotes mechanical time delay which is required by the motor driver unit to change the tap position by only one step and b is the control signal that is applied to the tap-changing mechanism (see **Figure 2**) and is given by

$$b = \begin{cases} 0 & \text{for } t \leq T_d : e = \text{arbitrary} \\ 1 & \text{for } t > T_d : e = 1 \\ -1 & \text{for } t > T_d : e = -1 \end{cases} \quad (5)$$

where T_d is the time delay introduced by the OLTC controller and e is the output of the hysteresis controller, that is,

$$e = \begin{cases} 0 & \text{for } |\Delta V| \leq DB \\ 1 & \text{for } \Delta V > DB \\ -1 & \text{for } \Delta V < -DB \end{cases} \quad (6)$$

The mechanical time delay (T_m) has a constant value; usually, it varies from 3 to 10 seconds, and ΔV is the voltage error. In some models of the OLTC, the controller time delay (T_d) is considered constant:

$$T_d = \tau_0 \quad (7)$$

However, T_d is usually variable and depends on the voltage error and the controller's dead band DB [4]:

$$T_d = \tau_0 \frac{DB}{|\Delta V|} \quad (8)$$

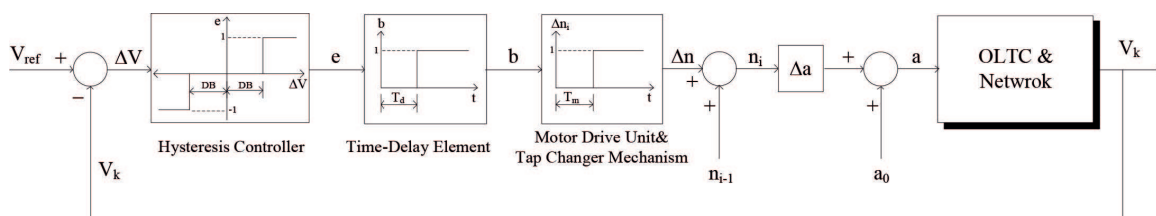


Figure 2.
 The schematic diagram of the conventional discrete control of the OLTC.

T_d is inversely proportional to the voltage error ΔV to avoid unnecessary operation during transient voltages and temporary load disturbances. DB must be greater than Δa to ensure stability when the regulated voltage approaches the reference value V_{ref} ; otherwise, the OLTC will suffer from hunting. V_{ref} is typically between 0.95 p.u. and 1.0 p.u. since it determines the steady-state voltage near the load center (V_k).

2.2 Conventional voltage control of inverter-based DGs

Energy processing strategies for inverter-based DGs typically involve two cascaded loops: inner and outer. The inner loop is a current control loop, which regulates the DG inverter current in the $d - q$ reference frame. The outer control loop, on the other hand, can fulfill different control objectives depending on the hosting grid, such as voltage regulation and power management control.

Figure 3 shows an inverter-based DG that is controlled in the current injection mode, which is the typical strategy adopted with RES. A DG inverter model in the $d - q$ synchronous frame represents the dynamics of the interfacing LC filter [5], that is,

$$L_f \frac{dI_d}{dt} = -R_f I_d + V_d - V_{od} + \omega L_f I_q \quad (9)$$

$$L_f \frac{dI_q}{dt} = -R_f I_q + V_q - V_{oq} - \omega L_f I_d \quad (10)$$

$$C_f \frac{dV_{od}}{dt} = I_d - I_{od} + \omega C_f V_{oq} \quad (11)$$

$$C_f \frac{dV_{oq}}{dt} = I_q - I_{oq} - \omega C_f V_{od} \quad (12)$$

$$\omega = \frac{d\theta}{dt} \quad (13)$$

where I_{dq} and I_{odq} represent the $d - q$ components of the inverter output current and DG current at the PCC, respectively; V_{dq} and V_{odq} are the components of the

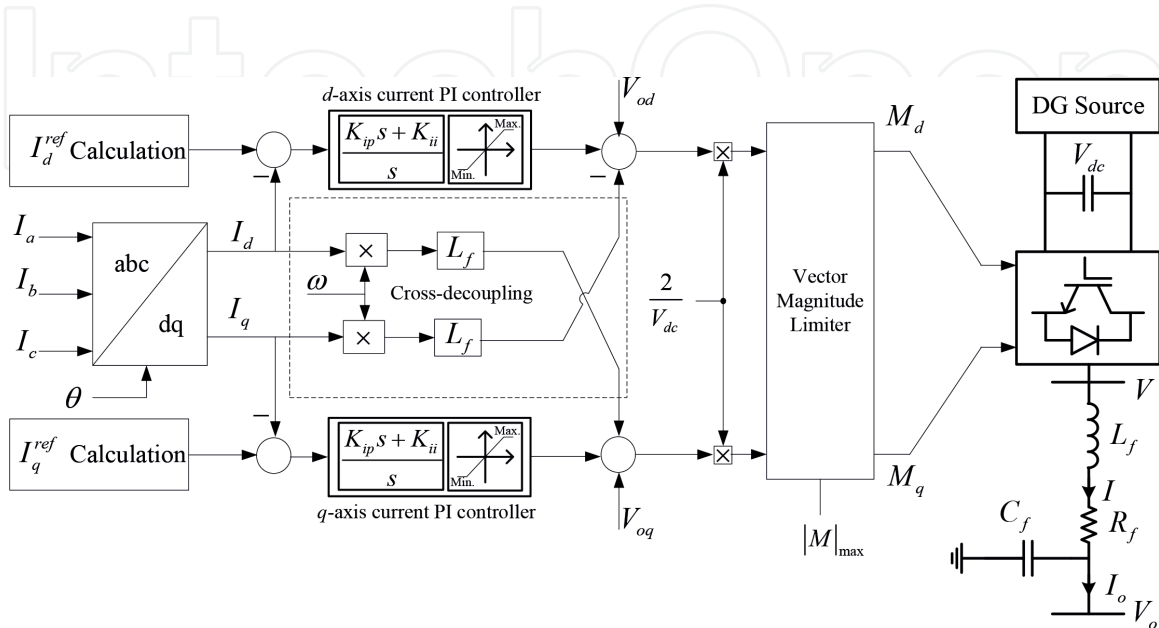


Figure 3.
Power circuit and current control diagram for inverter-based DG.

inverter terminal voltage and DG voltage at the PCC, respectively; R_f , L_f , and C_f are the resistance, inductance, and capacitance of the DG interfacing filter, respectively; and ω is the grid frequency.

The current equations, that is, (9) and (10), are coupled through the $\omega L_f I_q$ and $-\omega L_f I_d$ terms. For independent control of both the I_d and I_q currents, the decoupled terms must be eliminated, which can be accomplished if new variables V'_d and V'_q are defined by

$$V'_d = V_d - V_{od} + \omega L_f I_q \quad (14)$$

$$V'_q = V_q - V_{oq} - \omega L_f I_d \quad (15)$$

Substituting from (14) and (15) into (9) and (10) yields.

$$L_f \frac{dI_d}{dt} = -R_f I_d + V'_d \quad (16)$$

$$L_f \frac{dI_q}{dt} = -R_f I_q + V'_q \quad (17)$$

Equations (16) and (17) represent decoupled first-order differential equations for I_d and I_q , respectively. Therefore, PI current controllers can be designed based on the transfer functions derived from (16) and (17). If the gains of the PI current controllers are selected as

$$\begin{cases} K_{ip} = \frac{L_f}{\tau_i} \\ K_{ii} = \frac{R_f}{\tau_i} \end{cases}, \quad (18)$$

then the equivalent closed-loop transfer functions for the current loops can be given by

$$\frac{I_d(s)}{I_d^{ref}(s)} = \frac{I_q(s)}{I_q^{ref}(s)} = \frac{1}{\tau_i s + 1} \quad (19)$$

where τ_i is the time constant of the closed-loop system. The vector magnitude of the reference current $\left(\sqrt{\left(i_d^{ref}\right)^2 + \left(i_q^{ref}\right)^2} \right)$ should be limited according to the maximum allowable current, typically 20% greater than the rated current of the inverter [5], in order to provide overcurrent protection. The vector magnitude of the modulation index $\left(|M| = \sqrt{M_d^2 + M_q^2} \right)$ should also be limited to $|M|_{\max} = 1.0$ p. u. so that DG operates in a linear modulation region. **Figure 3** shows the vector magnitude limiter, which implies a limit on the magnitude of $|M|$ without a change in the phase angle between M_d and M_q .

Determination of the reference currents, I_d^{ref} and I_q^{ref} , is usually affiliated to the DG output power. In the synchronous $d - q$ frame, the output active P_G and reactive Q_G powers are given by

$$P_G = 1.5(V_{od}I_d + V_{oq}I_q) \quad (20)$$

$$Q_G = 1.5(V_{oq}I_d - V_{od}I_q) \quad (21)$$

For decoupled control of the active and reactive powers, a phase-locked loop (PLL) should be used for aligning V_{od} with the output voltage of phase a so that $V_{oq} = 0$ [6]. To determine I_d^{ref} , a maximum power point tracking (MPPT) algorithm along with a DC link voltage controller is employed [7]. On the other hand, I_d^{ref} can be calculated, as in (22), to regulate the output reactive power, thus, providing voltage support.

$$I_d^{ref} = \frac{Q_G^{ref}}{1.5V_{od}} \quad (22)$$

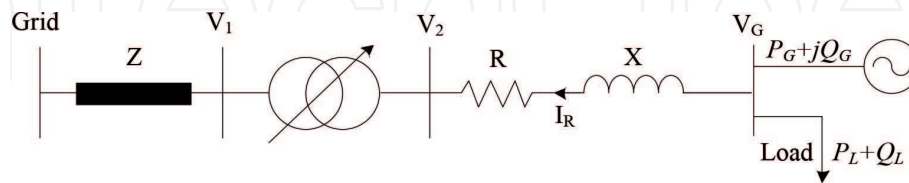
where Q_G^{ref} is the reference value of the DG reactive power which can be determined using an outer voltage control loop or received from a communication-assisted voltage regulation scheme [8].

2.3 DG contribution to voltage violation

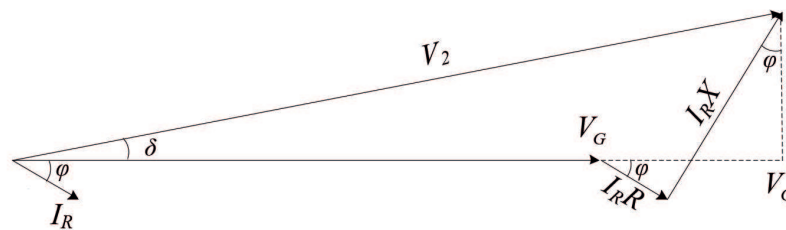
Usually, distribution networks have unidirectional power flow from the substation to customers. This leads to a descending voltage profile which may only suffer from an undervoltage near the load center, a problem typically tackled using OLTC and capacitor banks. On the other hand, DG integration into distribution networks makes the power flow bi-directional; thus an overvoltage problem may also occur. To understand the impact of DGs on the system voltage, the simplified distribution network in **Figure 4(a)** is used, where a DG is connected at a load bus. In this figure, R and X are the feeder resistance and reactance, respectively; I_R is the feeder current; V_b , V_2 are the primary and secondary voltage of the distribution transformer, respectively; and V_G is the DG output voltage. The phasor diagram of the simplified distribution network is shown in **Figure 4(b)**, in which δ is the power angle and φ is the phase shift between V_G and I_R .

Using the phasor diagram, the relation between the DG voltage and V_2 can be formulated:

$$\begin{aligned} V'_G &= [V_2 + I_R R \cos(\varphi) + I_R X \sin(\varphi)] \\ &= V_G \cos(\delta) \end{aligned} \quad (23)$$



(a)



(b)

Figure 4. Simplified distribution network with DG. (a) Single-line diagram and (b) phasor diagram.

The power angle (δ) is very small; hence (23) can be approximated by

$$V_G \approx V_2 + I_R R \cos(\varphi) + I_R X \sin(\varphi) \quad (24)$$

Therefore, the voltage rise caused by the DG, that is, $\Delta V_G = V_G - V_2$, is given by.

$$\Delta V_G \approx I_R R \cos(\varphi) + I_R X \sin(\varphi) = \frac{P_R R + Q_R X}{V_G} = \frac{(P_G - P_L)R + (Q_G - Q_L)X}{V_G} \quad (25)$$

where P_G and Q_G are the DG output active and reactive powers, respectively, while P_L and Q_L are the load active and reactive powers, respectively. It can be seen from (25) that the highest overvoltage happens when the DG generates its maximum power during a light load condition. This problem is mainly associated with the excessive reverse power flow caused by the DG.

3. Communication-assisted voltage regulation

Due to the intermittency of RES and PEVs, the conventional control schemes for OLTC and DGs fail to provide proper voltage regulation. This shortcoming can be compensated using communication-assisted voltage regulation schemes. In the literature, the communication-assisted schemes fall under two approaches: distributed and centralized [3]. Both approaches involve investment in communication links and remote terminal units. The distributed (intelligent) approach is considered to be an expert-based control or model-free approach, which coordinates a variety of voltage control devices with the goal of providing effective and nonoptimal voltage regulation with fewer communication requirements [9]. On the other hand, the centralized approach relies on a central point that monitors the system status and optimizes the operation of voltage control equipment. Typically, a centralized optimization problem is solved to dispatch the reactive power of different voltage control equipment based on (i) load forecasting and (ii) generation monitoring. Several solutions have been proposed in the literature to provide optimal reactive power dispatch for DGs [10–12]. In this section, the role of PEVs in optimal voltage regulation is explained as in [13].

3.1 PEV impact on voltage regulation

Figure 5 represents a simplified multi-feeder distribution network connected to a substation through an OLTC. The test network has a photovoltaic (PV)-based DG and a PEV parking lot, which are connected at different feeder terminals. Following the derivation of (25), the per-unit voltage deviation for both DG and PEV busses can be approximated by

$$\begin{aligned} \Delta V_{PV} &\approx (P_{PV} - P_{L_1})R_{f_1} + (Q_{PV} - Q_{L_1})X_{f_1} \\ \Delta V_{EV} &\approx -(P_{EV} + P_{L_2})R_{f_2} - (Q_{EV} + Q_{L_2})X_{f_2} \end{aligned} \quad (26)$$

where P_{PV} , P_{EV} , and P_L are DG, PEV, and load active powers, respectively, and Q_{PV} , Q_{EV} , and Q_L are DG, PEV, and load reactive powers, respectively.

Equation (26) shows that two worst-case scenarios may occur: (i) overvoltage, when the DG generates its maximum power during light loads and (ii) undervoltage, during a peak load demand and low DG output. The integration

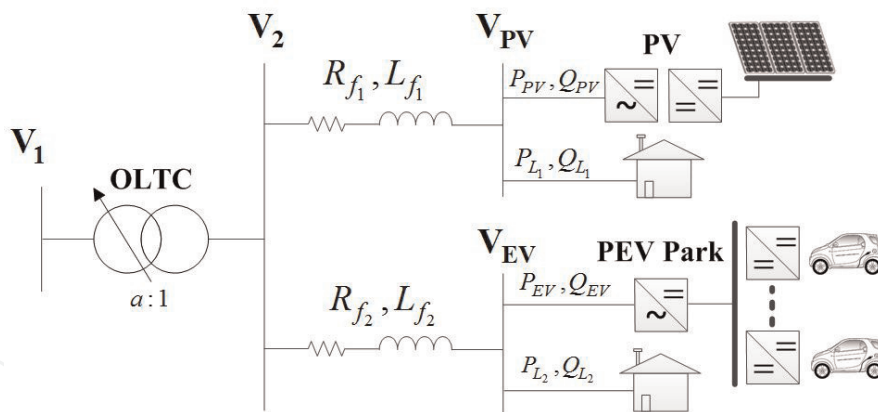


Figure 5.
Simplified distribution network with DG and PEVs.

of DGs changes the voltage profile significantly and complicates the voltage regulation. This is due to two reasons: (i) the voltage trend not descending from the substation to the feeder terminal, thereby invalidating the target point (reference) and (ii) the voltage estimation, based on local measurements, becoming inaccurate because of the stochastic power natures of RES and EVs [13]. Moreover, the stochastic power nature of EVs makes the voltage estimation inferior and aggravates the undervoltage problem. Therefore, OLTCs may suffer from wear and tear due to excessive operations. This problem worsens when feeders suffer from overvoltage due to high DG penetration, while others suffer from undervoltage during high demand, such as PEV charging. In this instance, the OLTC will have two contradicting solutions. Increasing the transformer's secondary voltage mitigates the undervoltage problem at the expense of the system's overvoltage and vice versa. **Figure 6** shows two daily power profiles for uncontrolled¹ PEV charging demand and a PV-based DG. The PEV demand is generated based on practical arrival/departure times from the Toronto Parking Authority (TPA), Toronto, Canada. Since the power profiles of commercial parking lots and PV-based DGs naturally coincide, there is a high chance that the system simultaneously suffers from overvoltage and undervoltage. A partial solution for this problem can be realized if a centralized-based controller for the OLTC exploits the system's maximum and minimum voltages. However, this controller may not prevent the OLTC hunting

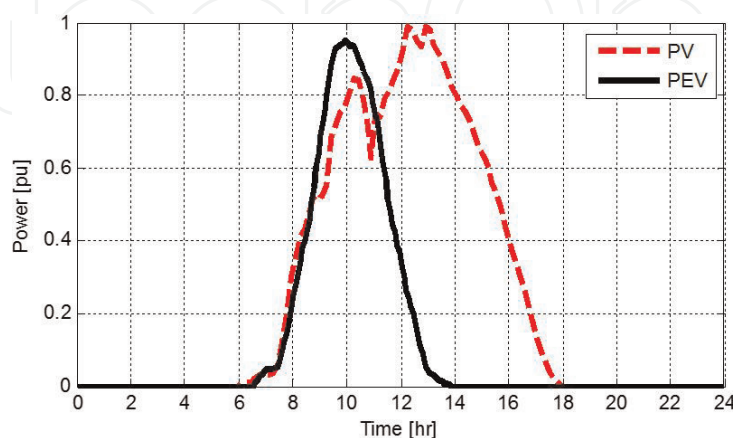


Figure 6.
DG and PEV power profiles.

¹ In uncontrolled charging schemes, PEVs start charging as soon as they are plugged in.

problem during high PV power generation and peak EV demand, resulting in excessive tap operation.

For that reason, the power electronic converters that interface DGs and PEVs should be utilized in voltage regulation. The DG can support the voltage regulation through two options: (i) absorbing reactive power and/or (ii) curtailment of active power. The first option is preferred since active power curtailment represents an energy waste. However, the capacity of the DG converter may limit the reactive power support and force the second option. To increase the reactive power support, the interfacing converter of the PEV can be employed to inject its surplus reactive power, thus reducing the DG active power curtailment [13]. A novel optimal coordinated voltage regulation scheme is presented to coordinate PEV, DG, and OLTC to achieve optimal voltage regulation and satisfy the self-objectives of each voltage control device.

3.2 OLTC centralized control

As shown in **Figure 7**, the OLTC is represented by a π -circuit model [14]. The taps are assumed to be at the primary side (high voltage). Subsequently, the OLTC secondary voltage and current can be calculated by

$$\begin{bmatrix} V_{(1,t)} \\ I_{(1,t)} \end{bmatrix} = \begin{bmatrix} 1 & -\frac{a}{Y_T} \\ \frac{1}{a} & -a \end{bmatrix} \begin{bmatrix} V_{(0,t)} \\ I'_{(0,t)} \end{bmatrix} \quad (27)$$

where Y_T is the transformer series admittance, a is the turns ratio given in (2), and t denotes the time instant. To take the physical busses into account, (27) can be rewritten as

$$\begin{bmatrix} I_{(0,t)} \\ I_{(1,t)} \end{bmatrix} = \underbrace{\begin{bmatrix} g_F + jb_\mu + \frac{Y_T}{a^2} & -\frac{Y_T}{a} \\ -\frac{Y_T}{a} & Y_T \end{bmatrix}}_{Y_{OLTC}} \begin{bmatrix} V_{(0,t)} \\ V_{(1,t)} \end{bmatrix} \quad (28)$$

where Y_{OLTC} is the OLTC Y-bus admittance matrix, which represents the OLTC admittance in the power flow equations.

The conventional OLTC controller, shown in **Figure 8(a)**, is modified to emulate an adaptive reference by considering the system's minimum and maximum voltages, that is, V_{\min}^{sys} and V_{\max}^{sys} , respectively. This modification forms the centralized OLTC controllers (COC) proposed in [13] and shown in **Figure 8(b)**, which

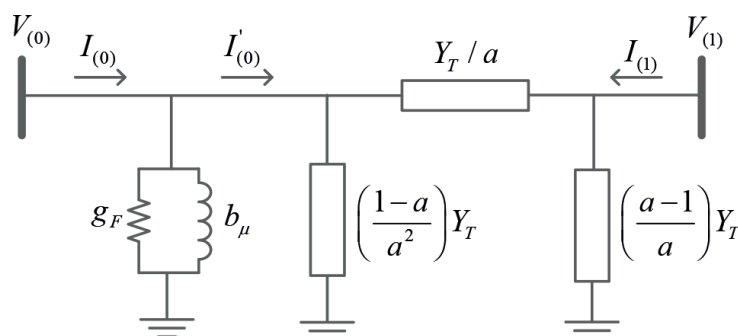


Figure 7.
 Equivalent π -circuit model of OLTC.

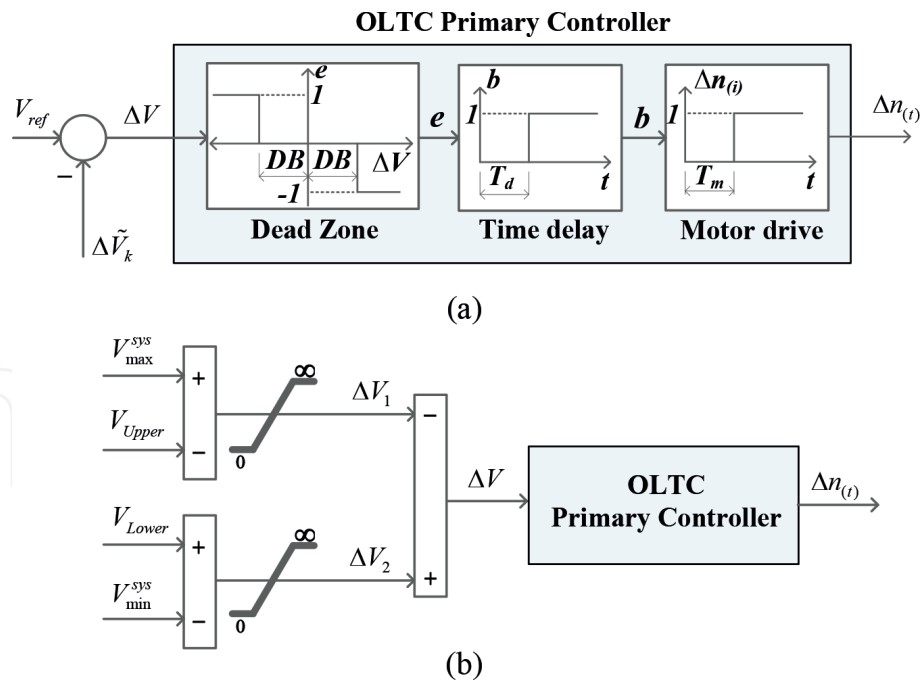


Figure 8. The OLTC control: (a) conventional local controller and (b) centralized OLTC controller (COC).

allows the OLTC to deal with multiple feeders with voltage problems resulted from DGs and PEVs. The COC emulates an adaptive reference because the error ΔV changes such that V_{\min}^{sys} and V_{\max}^{sys} are within the standard limits V_{Upper} and V_{Lower} (i.e., 1.05 and 0.95 p.u.), respectively. V_{\min}^{sys} and V_{\max}^{sys} can be estimated using the state estimation algorithm in [15] or attained through the central voltage control unit explained in the next subsection.

In the case of an overvoltage, ΔV is negative, and the primary controller decreases the transformer secondary voltage (by increasing the tap position) and vice versa. During normal conditions, ΔV is zero because both V_{\min}^{sys} and V_{\max}^{sys} are within the standard limits; thus, the tap position remains unchanged. When both overvoltage and undervoltage occur simultaneously, the COC should be disabled to avoid hunting [16]. In the next subsection, the roles of DGs and PEVs in voltage regulation are explained to mitigate the shortcoming of the COC.

3.3 Optimal coordinated voltage regulation

Both power electronic converters of PEVs and DGs can support the grid with reactive power to relax the OLTC. A vehicle-to-grid reactive power support (V2GQ) strategy is proposed in [13] to incorporate PEVs and DGs in voltage regulation, as shown in **Figure 9**. The main difference between vehicle-to-grid (V2G) strategies and the V2GQ is that the latter injects only reactive power to the grid. Thus, it preserves the battery life of PEV, that is, the highest priority of the vehicles' owners. Nevertheless, the V2GQ cannot be flexibly employed in power management because PEVs do not export active power to the grid. V2G strategies are avoided in voltage regulation to elongate the battery life, which is considered a priority in this study. The V2GQ comprises a three-stage nonlinear programming, in which Stage (I) aims at maximizing the energy delivered to PEVs, Stage (II) minimizes the DG active power curtailment, and Stage (III) minimizes the voltage deviations. The COC is coordinated such that it acts after Stage (III) to ensure that all bus voltages are within the standard limits.

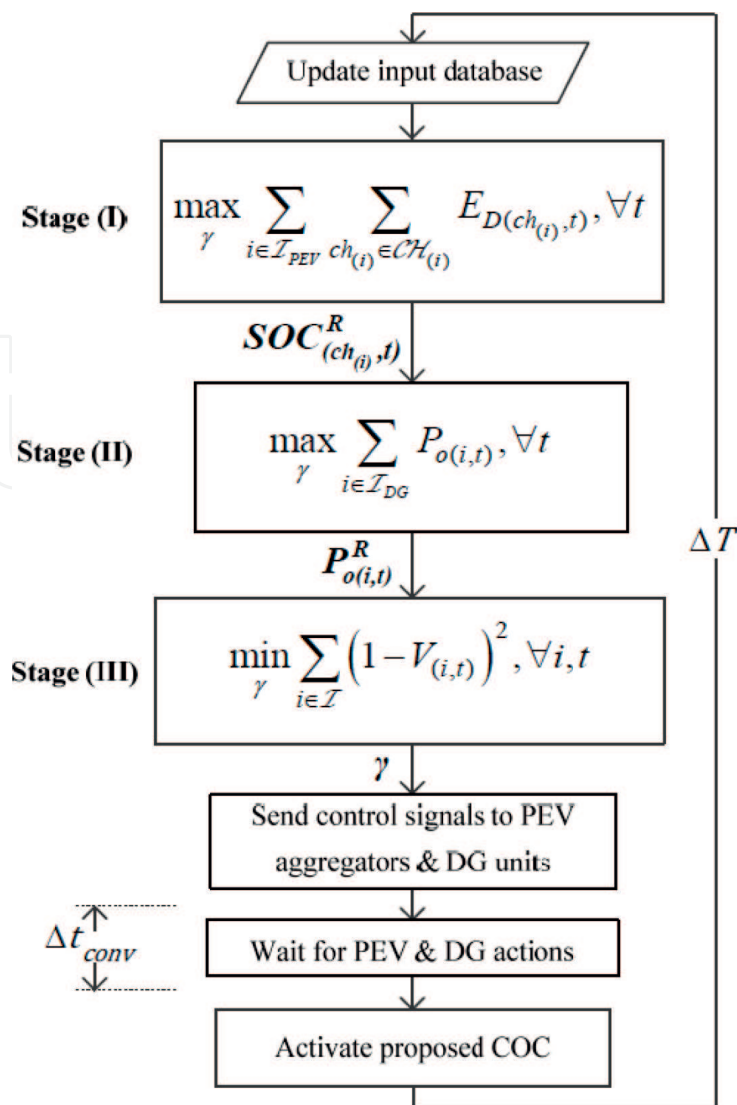


Figure 9.
 PEV/DG voltage support scheme.

3.3.1 Problem formulation of stage (I)

The main objective of Stage (I) is maximizing the energy delivered to PEV owners, that is,

$$\max_{\gamma} \sum_{i \in \mathcal{I}_{PEV}} \sum_{ch_{(i)} \in \mathcal{CH}_{(i)}} E_{D(ch_{(i)}, t)} \quad \forall t \quad (29)$$

where $E_{D(ch_{(i)}, t)}$ is the energy delivered to the PEV connected to charger $ch_{(i)} \in \mathcal{CH}_{(i)}$ at PEV bus $i \in \mathcal{I}_{PEV}$, \mathcal{I}_{PEV} is the set of busses with PEV charger connections, $\mathcal{CH}_{(i)}$ is the set of chargers connected to bus i , and γ is the decision variable vector. The PEV and DG voltage support depends mainly on γ , which can generally take the following form:

$$\gamma = \left[\mathbb{X}_{(ch_{(i)}, t)}, Q_{o(i,t)}^{PEV}, P_{o(i,t)}, Q_{o(i,t)} \right] \quad (30)$$

where $\mathbb{X}_{(ch_{(i)}, t)}$ and $Q_{o(i,t)}^{PEV}$ are the vector of the charger decisions and PEV reactive power at bus $i \in \mathcal{I}_{PEV}$, respectively; $P_{o(i,t)}$ and $Q_{o(i,t)}$ are the DG active and reactive powers at bus $i \in \mathcal{I}_{DG}$, respectively; and \mathcal{I}_{DG} is the set of busses with DG

connections. The charging decisions are continuous, that is, $\mathbb{X} \in [0, 1]$ where “0” stands for no charging and “1” stands for full charging. According to the grid operator, γ can be partially constrained. For instance, the PEV reactive powers can be set to zero, that is, $Q_{o(i,t)}^{PEV} = 0, \forall i \in \mathcal{I}_{PEV}, t$, when the PEV voltage support is disregarded. Stage (I) should satisfy the power flow constraints, as given by

$$P_{G(i,t)} - P_{L(i,t)} = \sum_{j \in \mathcal{I}_b} V_{(i,t)} V_{(j,t)} Y_{(ij)} \cos(\theta_{(ij)} + \delta_{(j,t)} - \delta_{(i,t)}) \quad \forall i \in \mathcal{I}_b, t \quad (31)$$

$$Q_{G(i,t)} - Q_{L(i,t)} = \sum_{j \in \mathcal{I}_b} V_{(i,t)} V_{(j,t)} Y_{(ij)} \sin(\theta_{(ij)} + \delta_{(j,t)} - \delta_{(i,t)}) \quad \forall i \in \mathcal{I}_b, t \quad (32)$$

where $P_{G(i,t)}$ and $Q_{G(i,t)}$ denote the generated active and reactive powers, respectively; $P_{L(i,t)}$ and $Q_{L(i,t)}$ are the active and reactive power demands, respectively; $V_{(i,t)}$ and $\delta_{(i,t)}$ denote the magnitude and angle of the voltage, respectively; \mathcal{I}_b is the set of system busses; and $Y_{(ij)}$ and $\theta_{(ij)}$ are the magnitude and angle of the Y-bus admittance matrix, respectively.

The voltage and feeder thermal limits should also hold, and thus,

$$V_{\min} \leq V_{(i,t)} \leq V_{\max}, \quad \forall i \in \mathcal{I}_b, t \quad (33)$$

$$I_{(l,t)} \leq I_{(l)}^{CAP}, \quad \forall l \in \mathcal{L}, t \quad (34)$$

where V_{\min} and V_{\max} are the maximum and minimum voltage limits, that is, 0.9 and 1.1 p.u., respectively; $I_{(l,t)}$ denotes the per-unit current through line $l \in \mathcal{L}$; \mathcal{L} is the set of system lines; and $I_{(l)}^{CAP}$ is the current carrying capacity.

Typically, two back-to-back power electronic converters are used to interface PEVs and PVs, that is, DC/DC and DC/AC converters. The DC/DC converter performs MPPT with PV-based DGs or controls the PEV charging. The DC/AC converter regulates the DC link voltage and is responsible for the reactive power support [7]. The power injected to a bus should be equal to the output power of the DG installed at that bus:

$$\begin{cases} P_{G(i,t)} = P_{o(i,t)} \\ Q_{G(i,t)} = Q_{o(i,t)} \end{cases}, \quad \forall i \in \mathcal{I}_{DG}, t \quad (35)$$

$$P_{o(i,t)} \leq P_{o(i,t)}^{MPPT}, \quad \forall i \in \mathcal{I}_{DG}, t \quad (36)$$

where $P_{o(i,t)}^{MPPT}$ denotes the DG maximum power available. In both PEVs and PVs, the DC/AC converter is similar to that used with Typ. 4 wind farms. Therefore, the reactive power capability limits, defined in [17], should be used as constraints. These limits depend on the converter's power rating and DC link voltage, as follows:

$$Q_{o(i,t)}^2 \leq S_{o(i,t)}^2 - P_{o(i,t)}^2, \quad \forall i \in \mathcal{I}_{DG}, t \quad (37)$$

$$\left(Q_{o(i,t)} + \frac{V_{(i,t)}^2}{X_{(i)}} \right)^2 \leq \left(\frac{V_{c(i)}^{\max} V_{(i,t)}}{X_{(i)}} \right)^2 - P_{o(i,t)}^2, \quad \forall i \in \mathcal{I}_{DG}, t \quad (38)$$

where $V_{c(i)}^{\max}$ represents the maximum converter voltage which depends on the converter DC link voltage [17, 18], $S_{o(i,t)}$ denotes the DG rated power, and $X_{(i)}$ is the total reactance of the DG filter and interfacing transformer at bus i . If the DC/AC converter increases the set point for the DC link voltage to relax Constraint (38), the DC/DC converter will operate at a high duty cycle, which decreases its efficiency [19]. Hence, the reactive power support from the DC/AC converter is limited by the DC link voltage.

The load power at a bus should be equal to the total power consumed by regular loads and PEV:

$$P_{L(i,t)} = P_{NL(i,t)} + P_{o(i,t)}^{PEV}, \quad \forall i \in \mathcal{I}_b, t \quad (39)$$

$$Q_{L(i,t)} = Q_{NL(i,t)} + Q_{o(i,t)}^{PEV}, \quad \forall i \in \mathcal{I}_b, t \quad (40)$$

where $P_{o(i,t)}^{PEV}$ is the PEV active power and $P_{NL(i,t)}$ and $Q_{NL(i,t)}$ are the active and reactive powers of normal loads, respectively. The PV power profile relies mainly on solar insolation, whereas $P_{o(i,t)}^{PEV}$ depends on charging decisions $\mathbb{X}_{(ch(i),t)}$, the charging power limit in kW $P_{CH(ch(i),t)}$, and the charging efficiency $\eta_{CH(ch(i),t)}$, as given by.

$$P_{o(i,t)}^{PEV} = \sum_{ch(i) \in \mathcal{CH}(i)} \frac{\mathbb{X}_{(ch(i),t)} P_{CH(ch(i),t)}}{\eta_{CH(ch(i),t)} S_{base}}, \quad \forall i \in \mathcal{I}_{PEV}, t \quad (41)$$

where S_{base} is the base power for the per-unit system in kW. The charging power limit P_{CH} is a function of the PEV battery state of charge (SOC) and is limited by the capacity of the charger, that is, $P_{CH} \leq P_{rated}^{Charger}$. This function is dependent on the characteristics of the battery, which can be expressed as

$$P_{CH(ch(i),t)} = f_{(ch(i),t)} \left(SOC_{(ch(i),t)}^F \right), \quad \forall i \in \mathcal{I}_{PEV}, ch(i), t \quad (42)$$

where $f_{(ch(i),t)}$ is the function that represents the characteristics of the PEV battery and $SOC_{(ch(i),t)}^F$ is the reached SOC. The relationship between the energy delivered to a PEV battery and its SOC can be given by

$$E_D(ch(i),t) = E_{BAT(ch(i))} \times \frac{\left(SOC_{(ch(i),t)}^F - SOC_{(ch(i),t)}^I \right)}{100}, \quad \forall i \in \mathcal{I}_{PEV}, ch(i), t \quad (43)$$

where $E_{BAT(ch(i))}$ is the battery capacity in kWh and $SOC_{(ch(i),t)}^I$ denotes the PEV initial SOC. The SOC of different PEVs are updated according to

$$SOC_{(ch(i),t)}^F = SOC_{(ch(i),t)}^I + \frac{\mathbb{X}_{(ch(i),t)} P_{CH(ch(i),t)} \left(\frac{\Delta T}{60} \right)}{E_{BAT(ch(i))}}, \quad \forall i \in \mathcal{I}_{PEV}, ch(i), t \quad (44)$$

where ΔT is the time step to collect the system data, run the program, and implement the decisions. Similar to DGs, the injected reactive powers from the PEVs should be limited by their converter ratings and DC link voltages, as given by

$$\left(Q_{o(i,t)}^{PEV}\right)^2 \leq \left(S_{o(i,t)}^{PEV}\right)^2 - \left(P_{o(i,t)}^{PEV}\right)^2, \quad \forall i \in \mathcal{I}_{PEV}, t \quad (45)$$

$$\left(Q_{o(i,t)}^{PEV} + \frac{V_{(i,t)}^2}{X_{(i)}}\right)^2 \leq \left(\frac{V_{c(i)}^{\max} V_{(i,t)}}{X_{(i)}}\right)^2 - \left(P_{o(i,t)}^{PEV}\right)^2, \quad \forall i \in \mathcal{I}_{PEV}, t \quad (46)$$

where $S_{o(i,t)}^{PEV}$ is the rated power of the PEV converter. In addition, the final achieved SOC, that is, $SOC_{(ch(i),t)}^F$, should be limited by the SOC desired by the PEV owners $SOC_{(ch(i),t)}^D$:

$$SOC_{(ch(i),t)}^F \leq SOC_{(ch(i),t)}^D, \quad \forall i \in \mathcal{I}_{PEV}, ch_{(i)}, t \quad (47)$$

3.3.2 Problem formulation of stage (II)

In Stage (II), the objective is to minimize the DG active power curtailment, where the final SOC reached in Stage (I), that is, $SOC_{(ch(i),t)}^R$, must be attained to ensure maximum customer satisfaction, which is the highest priority of the V2GQ technology. Therefore, this stage is subject to all of the constraints in Stage (I) except for (47), which is replaced by

$$SOC_{(ch(i),t)}^F = SOC_{(ch(i),t)}^R, \quad \forall i \in \mathcal{I}_{PEV}, ch_{(i)}, t \quad (48)$$

Thus, the objective function of Stage (II) is

$$\max_{\gamma} \sum_{i \in \mathcal{I}_{DG}} P_{o(i,t)}, \quad \forall t \quad (49)$$

3.3.3 Problem formulation of stage (III)

Stage (III) aims at minimizing the voltage deviation using the DGs and PEVs to restore a feasible solution for the COC and relax the tap operation. Thus,

$$\min_{\gamma} \sum_{i \in \mathcal{I}_b} (1 - V_{(i,t)})^2, \quad \forall i, t \quad (50)$$

Besides all the constraints in Stage (II), this problem is subject to the constraint defined in (50), in which the maximum injected powers from the DGs reached in Stage (II), that is, $P_{o(i,t)}^R$, should be maintained.

$$P_{o(i,t)} = P_{o(i,t)}^R, \quad \forall i \in \mathcal{I}_{DG}, t \quad (51)$$

3.4 Coordination between V2GQ and COC

The charging decisions and active/reactive dispatch signals produced in Stage (III) are sent to all PEV parking lots and DGs, as shown in **Figure 9**. To ensure that the PEV and DG converters settle at the desired active and reactive power references, a time delay Δt_{conv} is introduced. The converter settling time may vary from 50 to 100 ms, depending on the primary controllers of the DC/AC converter [7]. For slow automatic interactions, such as voltage regulation, the maximum communication time delay is 100 ms as per the IEC 61850 [20]. Thus, Δt_{conv} is assumed to be

200 ms (100 ms for the converter settling time + 100 ms for the communication latency). Lastly, the COC refines the output solution from Stage (III) to ensure that both V_{\min}^{sys} and V_{\max}^{sys} are within the standard voltage limits. The total execution time of the coordination algorithm ΔT is 5 minutes.

3.5 Real-time results

In this section, various case studies are presented to validate the robustness and effectiveness of the optimal coordinated voltage regulation algorithm. The 38-bus 12.66-kV distribution system is used as a test system, as shown in **Figure 10**. The system data can be found in [21]. The system is modified to accommodate two PEV parking lots and four PV-based DGs, with power ratings as given in **Figure 10**. The power demands of the two parking lots are extracted from data provided by the TPA for a weekday in 2013. Both parking lots are commercial, where P1 represents a lot in the vicinity of a train station and P2 is a lot located near downtown Toronto. The total number of PEVs during a day is displayed in **Figure 11**. Due to confidentiality, the addresses of the real parking lots are not mentioned. The central control unit receives the desired SOCs and sends the charging decisions to all vehicles in the parking lots. An OPAL real-time simulator (RTS) is used to model the visual test network using the SimPowerSystems blockset, which is available in Simulink/Matlab, and an ARTEMiS plug-in [22]. The network, PEV, and DG models are

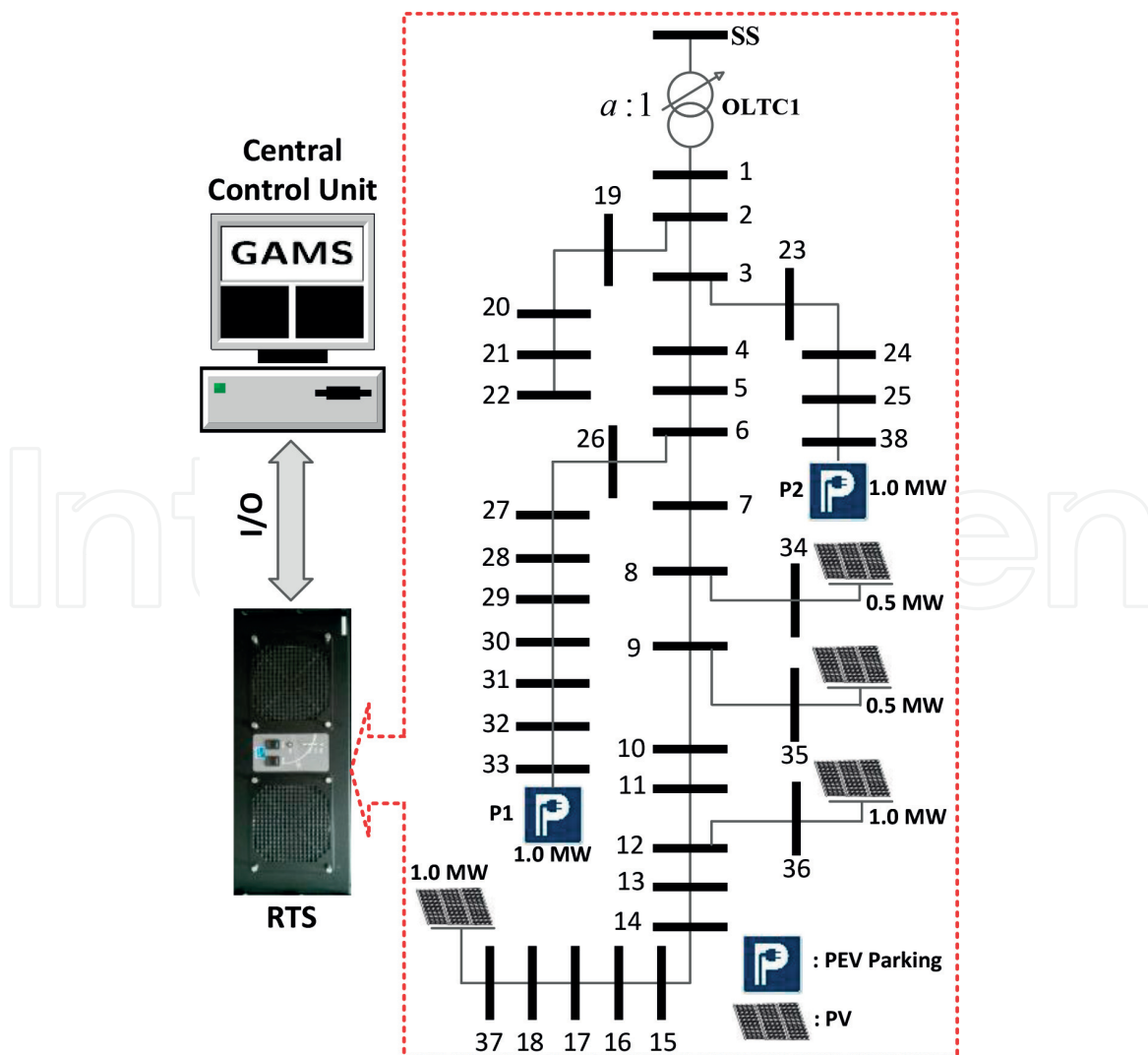


Figure 10.
 Test network with an HiL realization.

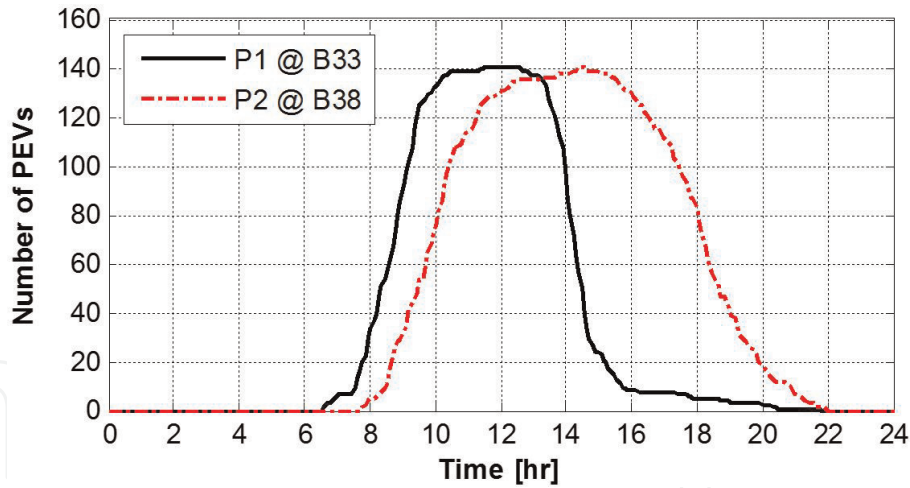


Figure 11.
Number of vehicles in the parking lots.

distributed between the RTS cores for performing parallel computations. The RTS is used to perform a hardware-in-the-loop (HiL) realization, where a central control unit, emulated by a host computer running GAMs, exchanges real-time data with the test network modeled in the RTS. The sampling time used to realize the HiL application is 100 μ s.

3.5.1 OLTC control without PEV/DG voltage support

This section compares the responses of the conventional and COC controllers for the OLTC. The voltage support from PEVs and DGs is disabled to study their

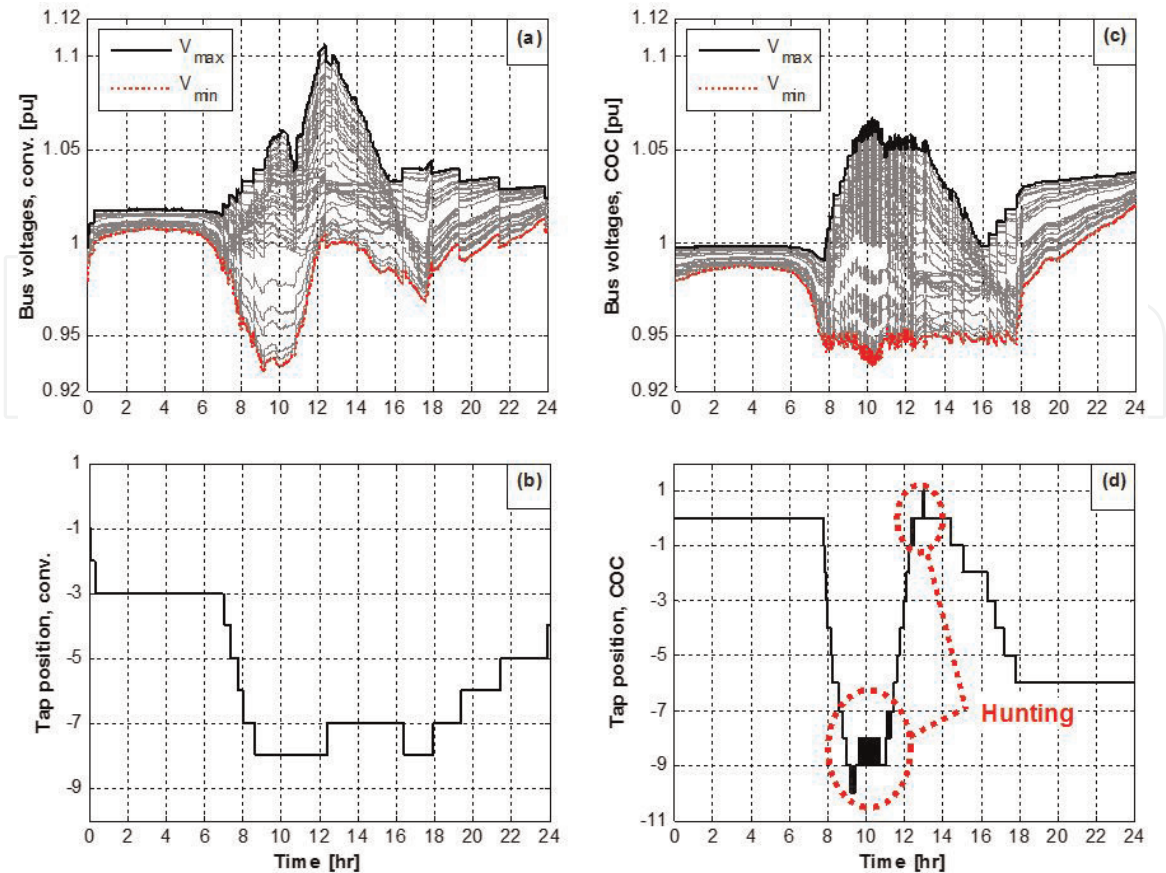


Figure 12.
OLTC response: (a & b) conventional control and (c & d) COC.

impacts of the OLTC. **Figure 12(a)** and **(b)** illustrate the response of the conventional controller for the OLTC over 24 hours. Although the OLTC does not suffer from an excessive tap operation (13 taps/day), undervoltage and overvoltage problems occur.

As expected, the overvoltage happens during the peak power generation from DGs, while the undervoltage coincides with the peak demand of PEV. The COC is enabled to mitigate these voltage violations. **Figure 12(c)** and **(d)** demonstrate that the COC can limit the voltage violations without the PEV/DG voltage support, but it suffers from a hunting problem. This problem happens when the overvoltage and undervoltage occur concurrently. In this situation, the COC should be deactivated.

3.5.2 OLTC control with PEV/DG voltage support

To address the hunting problem, presented in the previous case, the V2GQ is coordinated with the COC. Two case studies dealing with PEV/DG voltage support are carried out, as follows:

1. DG active power curtailment, without PEV and DG reactive power supports, that is, $\gamma = \left[\mathbb{X}_{(ch(i),t)}, P_{o(i,t)} \right]$, where $Q_{o(i,t)}^{PEV} = 0, \forall i \in \mathcal{I}_{PEV}$ and $Q_{o(i,t)} = 0, \forall i \in \mathcal{I}_{DG}$
2. PEV and DG reactive power dispatch, that is, $\gamma = \left[\mathbb{X}_{(ch(i),t)}, Q_{o(i,t)}^{PEV}, P_{o(i,t)}, Q_{o(i,t)} \right]$

Figure 13 demonstrates the performance of the coordination algorithm when the voltage support is merely achieved via the DG active power curtailment (i.e., the

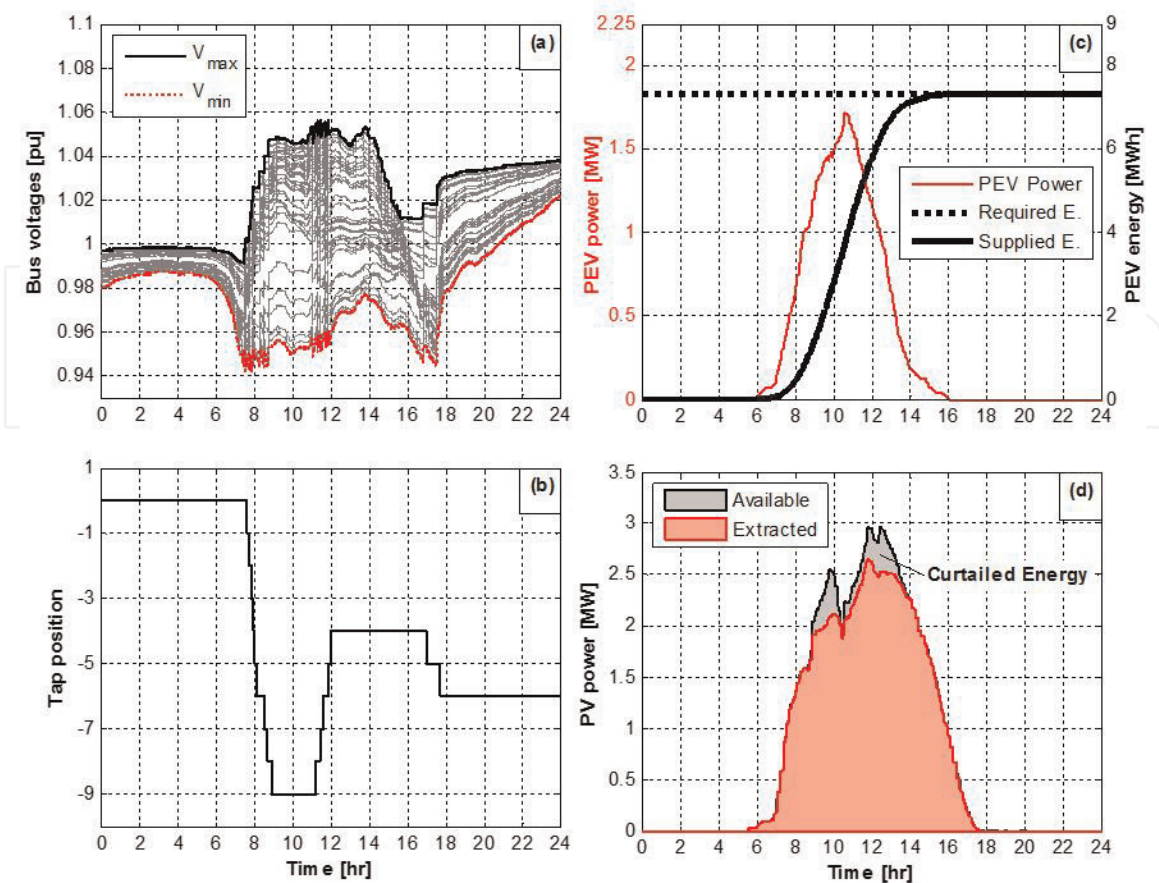


Figure 13.
 Response of coordination algorithm, assuming DG active power curtailment.

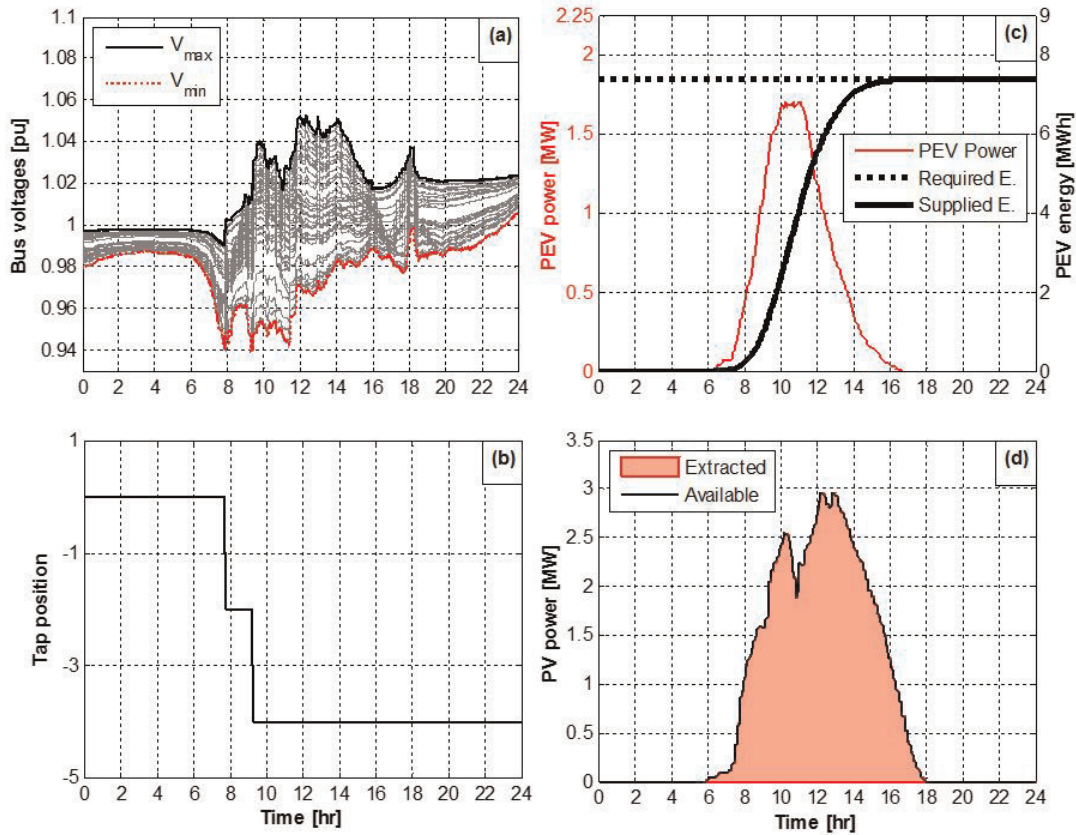


Figure 14. Response of coordination algorithm, activating both PEV and DG reactive power dispatch.

first case study). The coordination algorithm keeps the bus voltages within the standard limits, as shown in **Figure 13(a)**. The hunting problem is avoided with a reasonable daily tap operation, that is, 16 taps/day; see **Figure 13(b)**. Further, the required PEV charging demand is satisfied, as illustrated in **Figure 13(c)**. However, 6.14% of the DG available energy is curtailed because the priority is given to supplying the PEV demand, as shown in **Figure 13(d)**. This privilege is considered to comply with the distribution system code developed by the Ontario Energy Board [23]. It states that electric utilities should deliver the required energy to supply their loads (such as PEVs) unless there is a technical limit violation. The only solution to maximize the energy extraction is therefore to incorporate both the PEVs and DGs in the voltage support. **Figure 14** illustrates the response of the coordination algorithm for the second case when PEV and DG reactive powers are employed for voltage regulation. Utilizing the full features of the V2GQ results in a proper voltage regulation using only 4 taps/day, extracting all DG power and charging all PEVs.

4. Conclusion

This chapter explained the conventional voltage regulation schemes used in smart grids with inverter-based DGs and PEVs. High penetration levels of PEVs and DGs may lead to negative impacts on the conventional voltage control devices such as tap-changing transformers and capacitor banks. The main reason behind these negative impacts is the stochastic power profiles of PEVs and renewable-based DGs that stimulate chronological overvoltage and undervoltage and make load forecasting erroneous. In the literature, there are two approaches to mitigating the voltage


violations associated with DGs and PEVs: (i) centralized and (ii) distributed voltage regulation schemes. These schemes necessitate communication and, thus, may benefit from the communication infrastructure embedded within smart grids. The centralized approach employs state estimation and solves an optimization problem to dispatch DG reactive power for optimal voltage regulation. On the other hand, the distributed approach is an expert-based control or model-free approach, which coordinates a variety of voltage control devices with the goal of providing effective and nonoptimal voltage regulation with fewer communication requirements. Case studies for a centralized voltage control scheme illuminated the role of PEV and DG reactive powers in providing optimal voltage regulation with relaxed tap operation.

Author details

Maher Azzouz
University of Windsor, Windsor, Ontario, Canada

*Address all correspondence to: mazzouz@uwindsor.ca

IntechOpen

© 2019 The Author(s). Licensee IntechOpen. This chapter is distributed under the terms of the Creative Commons Attribution License (<http://creativecommons.org/licenses/by/3.0>), which permits unrestricted use, distribution, and reproduction in any medium, provided the original work is properly cited. 

References

- [1] Estimating the Costs and Benefits of the Smart Grid: A Preliminary Estimate of the Investment Requirements and the Resultant Benefits of a Fully Functioning Smart Grid. Palo Alto, CA: EPRI; 2011
- [2] The Smart Grid: An Estimation of the Energy and CO₂ Benefits. Pacific Northwest National Lab; 2010
- [3] Vovos PN, Kiprakis AE, Wallace AR, Harrison GP. Centralized and distributed voltage control: Impact on distributed generation penetration. *IEEE Transactions on Power Apparatus and Systems*. 2007;**22**(1):476-483
- [4] Faiz J, Siahkollah B. Differences between conventional and electronic tap-changers and modifications of controller. *IEEE Transactions on Power Delivery*. 2006;**21**(3):1342-1349
- [5] Zamani MA, Yazdani A, Sidhu TS. A control strategy for enhanced operation of inverter-based microgrids under transient disturbances and network faults. *IEEE Transactions on Power Delivery*. 2012;**27**(4):1737-1747
- [6] Karimi-Ghartemani M, Iravani MR. A method for synchronization of power electronic converters in polluted and variable-frequency environments. *IEEE Transactions on Power Apparatus and Systems*. 2004;**19**(3):1263-1270
- [7] Yazdani A, Iravani R. *Voltage-Sourced Converters in Power Systems*. Wiley-IEEE Press; Feb 2010. ISBN-10: 0470521562
- [8] Katiraei F, Iravani R, Hatziargyriou N, Dimeas A. Microgrids management. *The IEEE Power & Energy Magazine*. 2008;**6**(3):54-65
- [9] Azzouz MA, Farag HE, El-Saadany EF. Real-time fuzzy voltage regulation for distribution networks incorporating high penetration of renewable sources. *IEEE Systems Journal*. Sep 2017;**1**(3): 1702-1711
- [10] Daratha N, Das B, Sharma J. Coordination between OLTC and SVC for voltage regulation in unbalanced distribution system distributed generation. *IEEE Transactions on Power Apparatus and Systems*. 2013;**29**(1):1-11
- [11] Agalgaonkar YP, Pal BC, Jabr RA. Distribution voltage control considering the impact of PV generation on tap changers and autonomous regulators. *IEEE Transactions on Power Apparatus and Systems*. 2014;**29**(1):182-192
- [12] Bonfiglio A, Brignone M, Delfino F, Procopio R. Optimal control and operation of grid-connected photovoltaic production units for voltage support in medium-voltage networks. *The IEEE Transactions on Sustainable Energy*. 2014;**5**(1):254-263
- [13] Azzouz MA, Shaaban MF, El-Saadany EF. Real-time optimal voltage regulation for distribution networks incorporating high penetration of PEVs. *IEEE Transactions on Power Apparatus and Systems*. 2015;**30**(6)
- [14] Milano F. Hybrid control model of under load tap changers. *IEEE Transactions on Power Delivery*. 2011; **26**(4):2837-2844
- [15] Elkhateb ME, El-Shatshat R, Salama MMA. Novel coordinated voltage control for smart distribution networks with DG. *IEEE Transactions on Smart Grid*. 2011;**2**(4):598-605
- [16] Farag HE, El-Saadany EF, Seethapathy R. A two ways communication-based distributed control for voltage regulation in smart

distribution feeders. *IEEE Transactions on Smart Grid*. 2012;**3**(1):271-281

[17] Ullah NR, Bhattacharya K, Thiringer T. Wind farms as reactive power ancillary service providers—Technical and economic issues. *IEEE Transactions on Energy Conversion*. 2009;**24**(3): 661-672

[18] Zhou K, Wang D. Relationship between space-vector modulation and three-phase carrier-based PWM: A comprehensive analysis [three-phase inverters]. *IEEE Transactions on Industrial Electronics*. 2002;**49**(1): 186-196

[19] Kazimierczuk MK. *Pulse-Width Modulated DC-DC Power Converters*. John Wiley & Sons; 2008

[20] *Communication Networks and Systems in Substations—Part 5: Communication Requirements for Functions and Device Models*. IEC 61850-5 ed2; 2003

[21] Singh D, Misra RK, Singh D. Effect of load models in distributed generation planning. *IEEE Transactions on Power Apparatus and Systems*. 2007;**22**(4): 2204-2212

[22] Azzouz MA, El-Saadany EF. Multivariable grid admittance identification for impedance stabilization of active distribution networks. *IEEE Transactions on Smart Grid*. 2016:1-13. in press

[23] Ontario Energy Board. *Distribution system code*. 2013. Available from: <http://www.ontarioenergyboard.ca/OEB/Documents/Regulatory/DistributionSystemCode.pdf>